Supplement of Atmos. Chem. Phys., 22, 14147–14175, 2022
https://doi.org/10.5194/acp-22-14147-2022-supplement

Atmospheric Chemistry and Physics
Open Access
EGU

Supplement of

Chamber investigation of the formation and transformation of secondary organic aerosol in mixtures of biogenic and anthropogenic volatile organic compounds

Aristeidis Voliotis et al.

Correspondence to: Gordon McFiggans (g.mcfiggans@manchester.ac.uk)

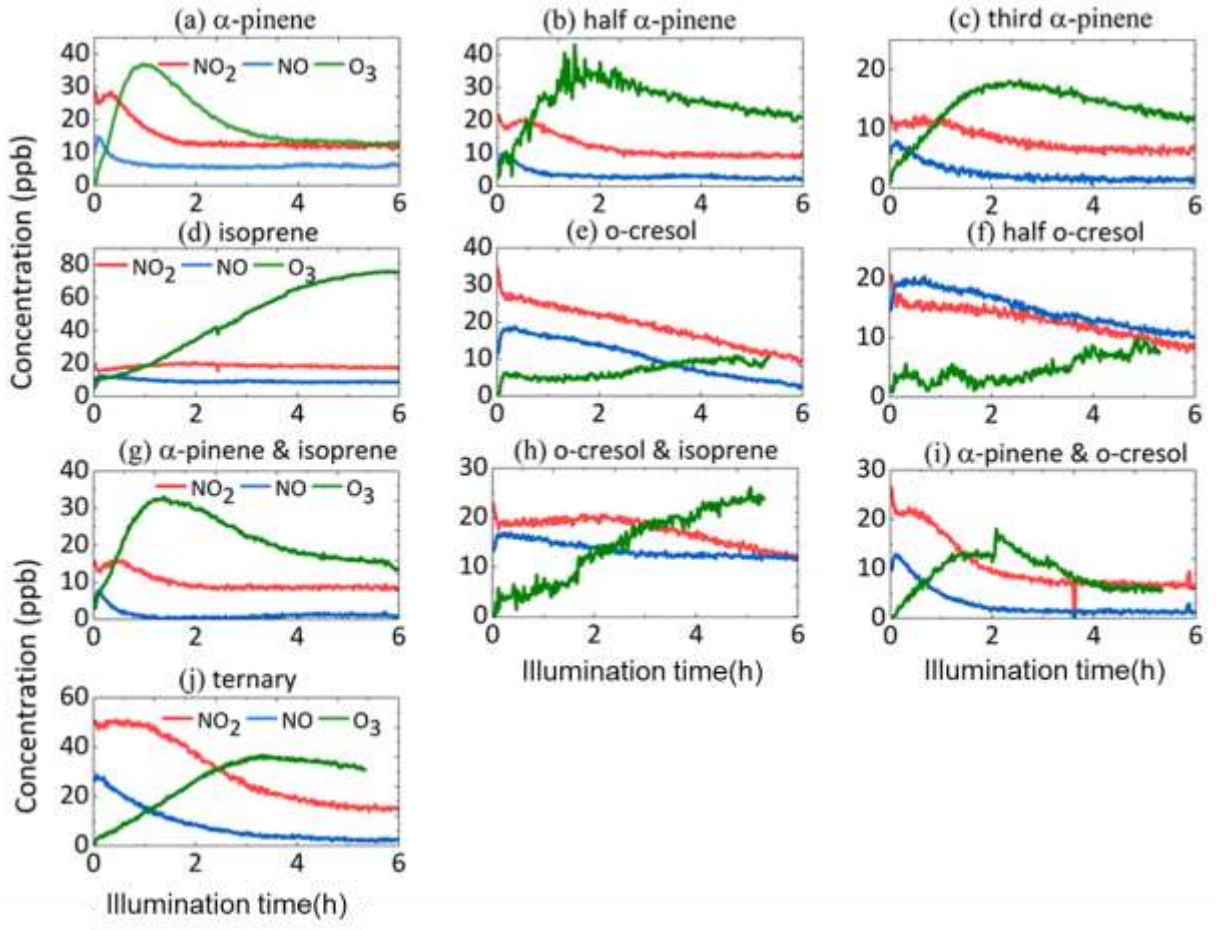

Figure S1: NO_2, NO and O_3 time series in all single and mixed VOC systems (example representative experiments). Note that, in the presence of *o*-cresol, O_3 measurement by UV absorption was influenced by UV absorption by *o*-cresol and O_3 data were corrected for all o-cresol containing systems as explained in the methods section.

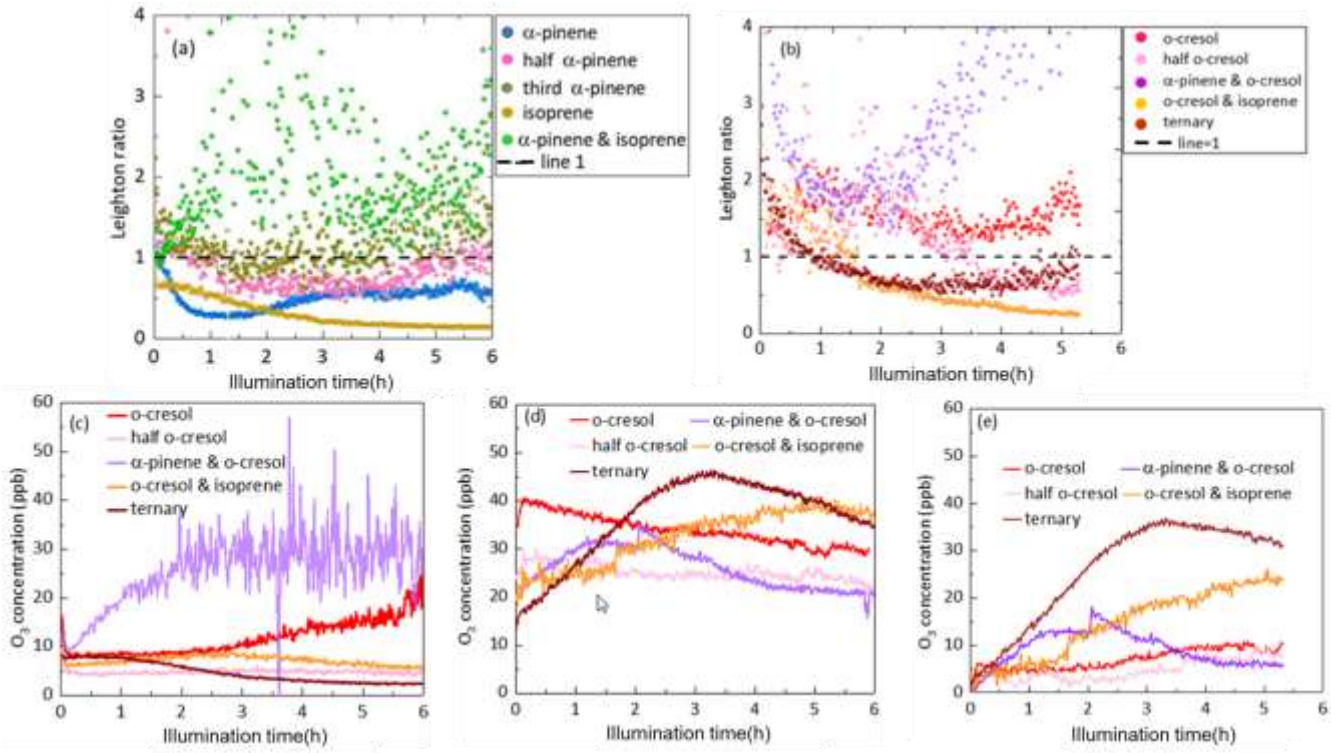

Figure S2: Leighton ratios in all systems and O_3 concentrations in all *o*-cresol containing systems. (a) Leighton ratio in all non-*o*-cresol containing systems, (b) Leighton ratio in all *o*-cresol containing systems, (c) O_3 concentrations calculated assuming PSS in the *o*-cresol containing systems, (d) measured O_3 concentrations from O_3 analyser in all *o*-cresol containing systems, (e) corrected O_3 concentrations based on CIMS *o*-cresol signal in all *o*-cresol containing systems.

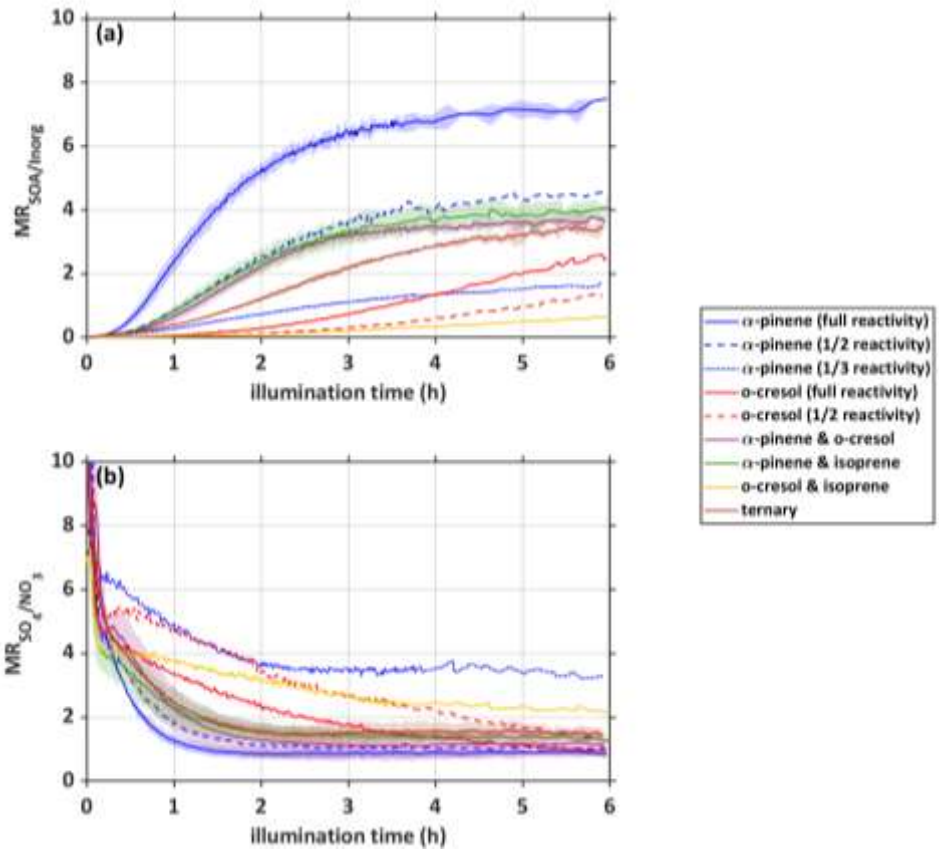

Figure S3: Total particle wall loss corrected particle component mass ratios in each system showing inorganic and organic component evolution and coloured consistently with Figures 2 and 3. Panel a) shows the increase in SOA : inorg ratio follows the production of SOA particle mass and the loss of total particle mass to the walls. In the wall loss correction, the size-resolved loss of multi-component organic-inorganic aerosol particles is assumed to be the same as that for size-resolved ammonium sulphate seeds loss rate measured in dedicated experiments (see methodology). Panel b) shows the decrease in SO_4^{2-}: NO_3^-, throughout the experiment in each system follows the wall loss of total particle mass (and hence SO_4^{2-}) and simultaneous oxidation of NO_2 by OH to form HNO_3 (and hence particulate NO_3^-). Note that NH_4^+ was found to ion balance the sum of NO_3^-:SO_4^{2-} in all experiments within measurement uncertainty

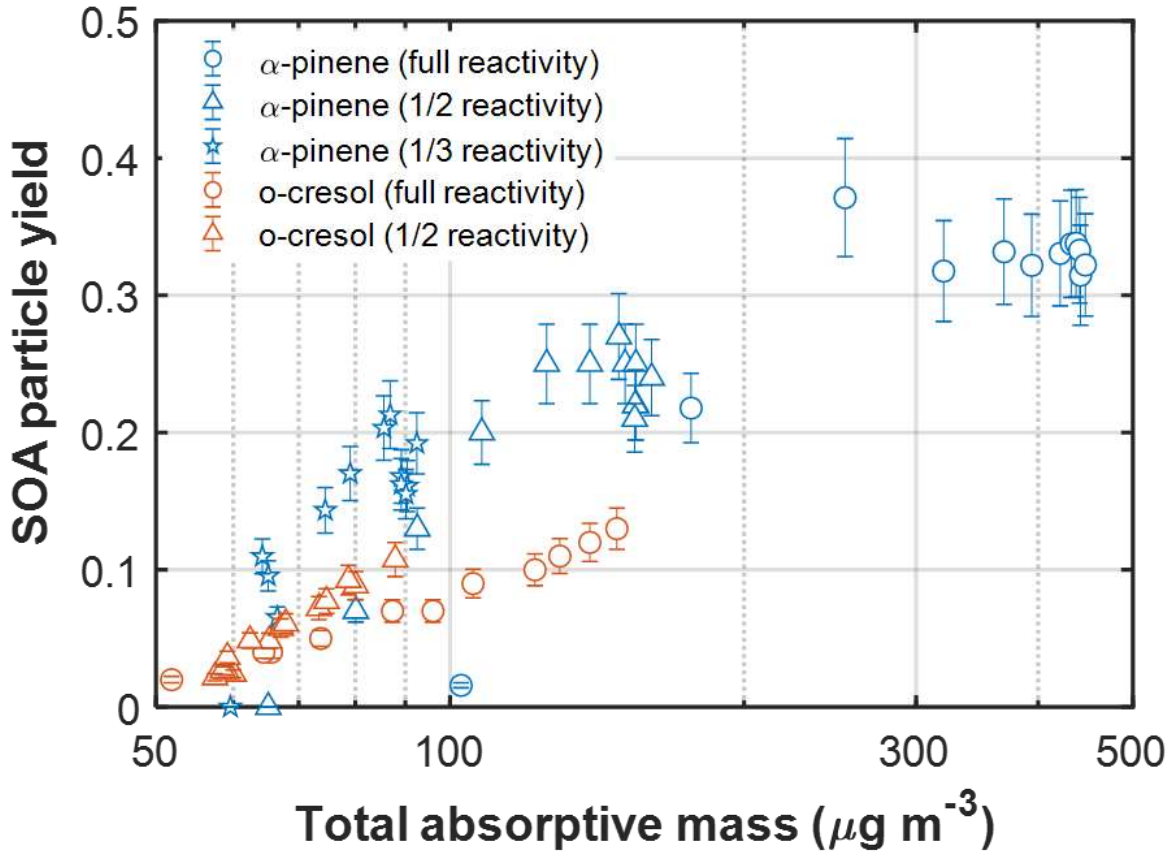

Figure S4: SOA particle mass yield as a function of total absorptive mass, including the remaining inorganic seed mass, in the single precursor α-pinene and *o*-cresol experiments at all initial concentrations. Error bars represent the propagated uncertainties in all measurements and in the particle wall loss corrections applied.

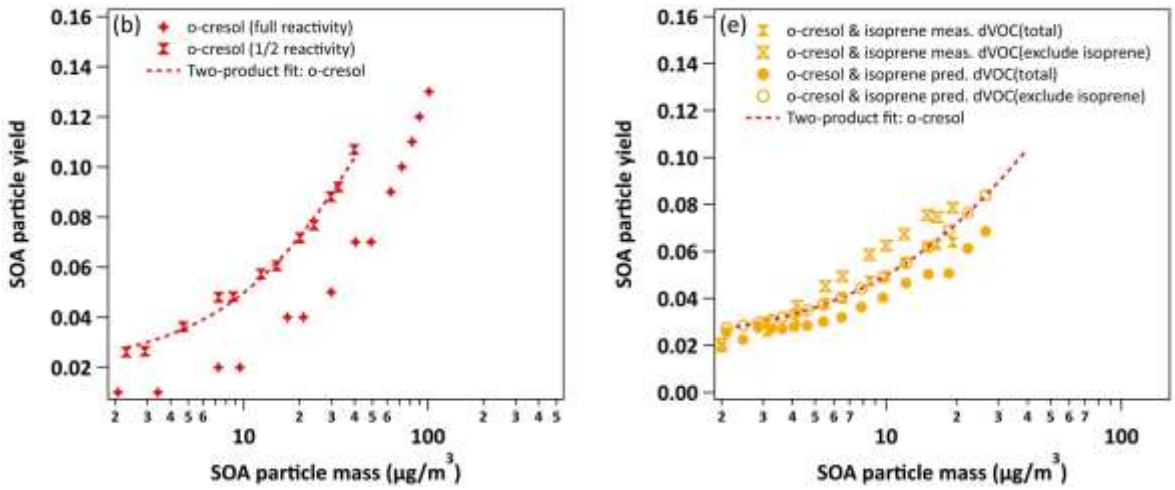

Figure S5: Expanded plot of yield data for the *o*-cresol / isoprene mixture (with 2-product yield curves *o*-cresol single VOC experiment). Yields "predicted" from the linear combination of yields from the individual VOC experiment using equation 4 are shown for the mixture.

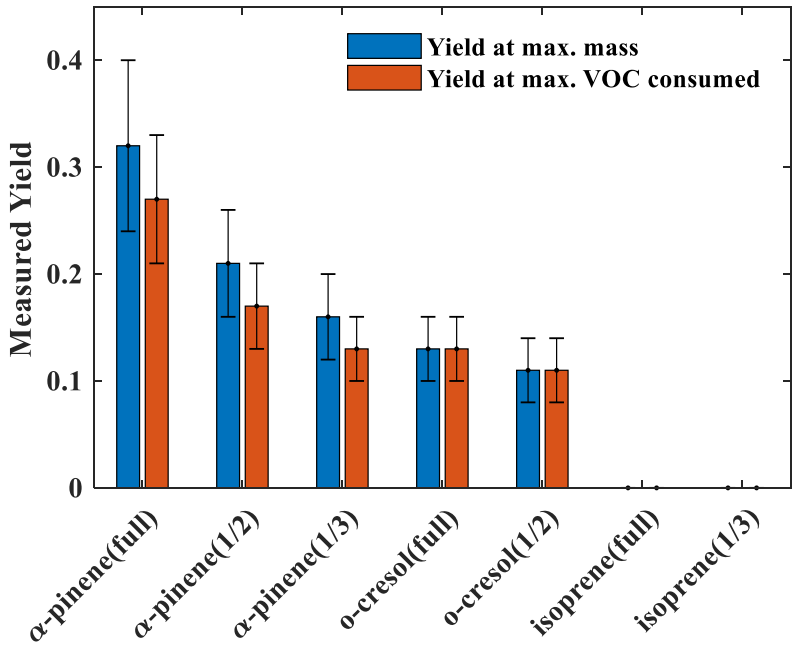

Figure S6: Measured yield for all single available precursor systems calculated at maximum particle mass and maximum VOC consumed

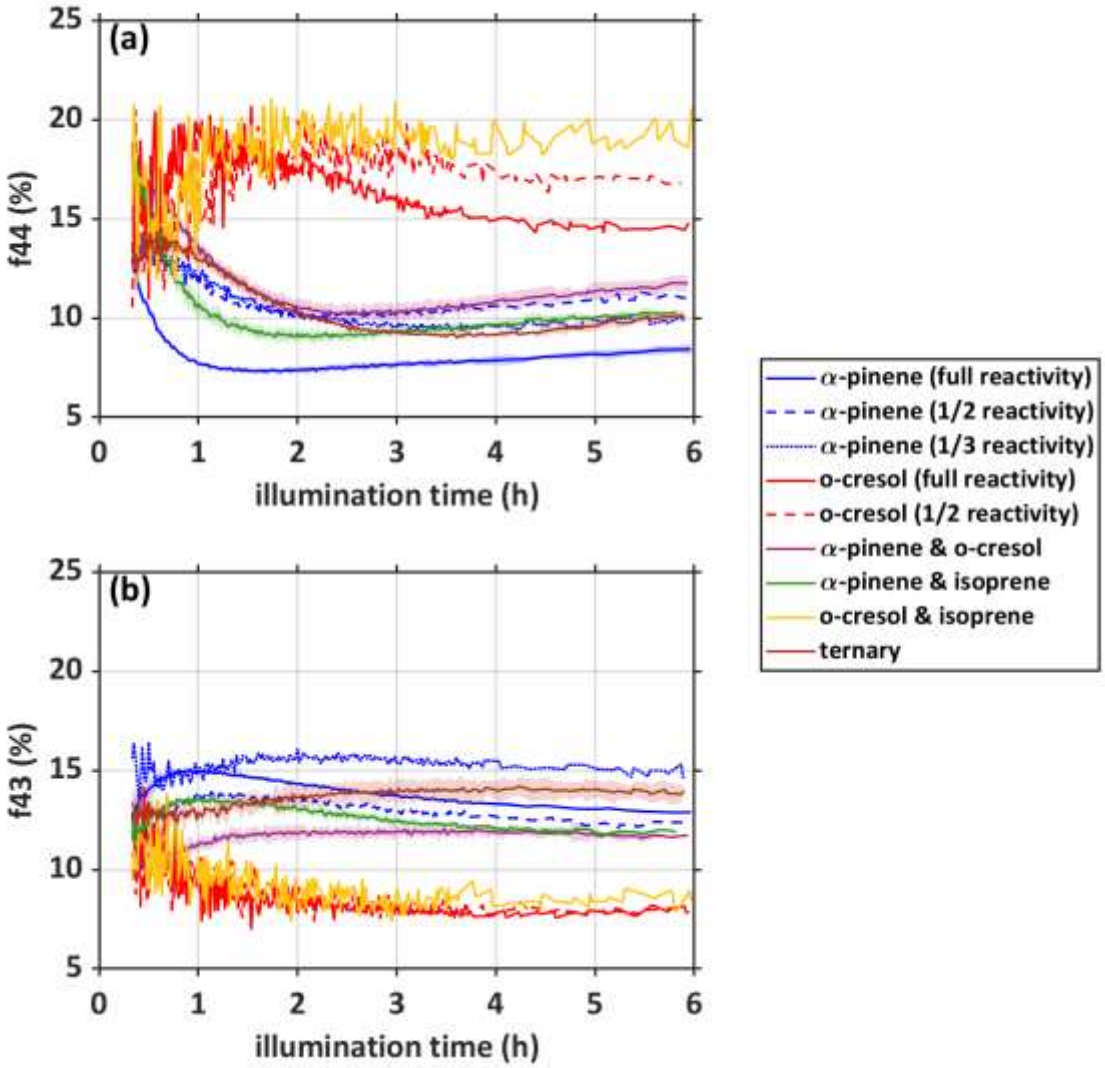

Figure S7: Time series of the signal fraction of m/z=44 (panel a) and m/z=43 (panel b) in total organic signal measured by AMS, representing more- and less-oxygenated contribution to total SOA particle mass in all systems explored in this study. *m/z*=44 is the CO_2^+ fragment formed by decarboxylation on the AMS vapouriser and *m/z*=43 corresponds to the presence of less oxidised components like carbonyls (with a small unsubtracted contribution from unoxidised alkyl fragment ions). The full reactivity single VOC α-pinene experiment has the lowest f_{44} and highest f_{43} of all systems. Systems that do not contain α-pinene can be seen to comprise a persistently higher f_{44} and lower f_{43} than all α-pinene-containing systems.

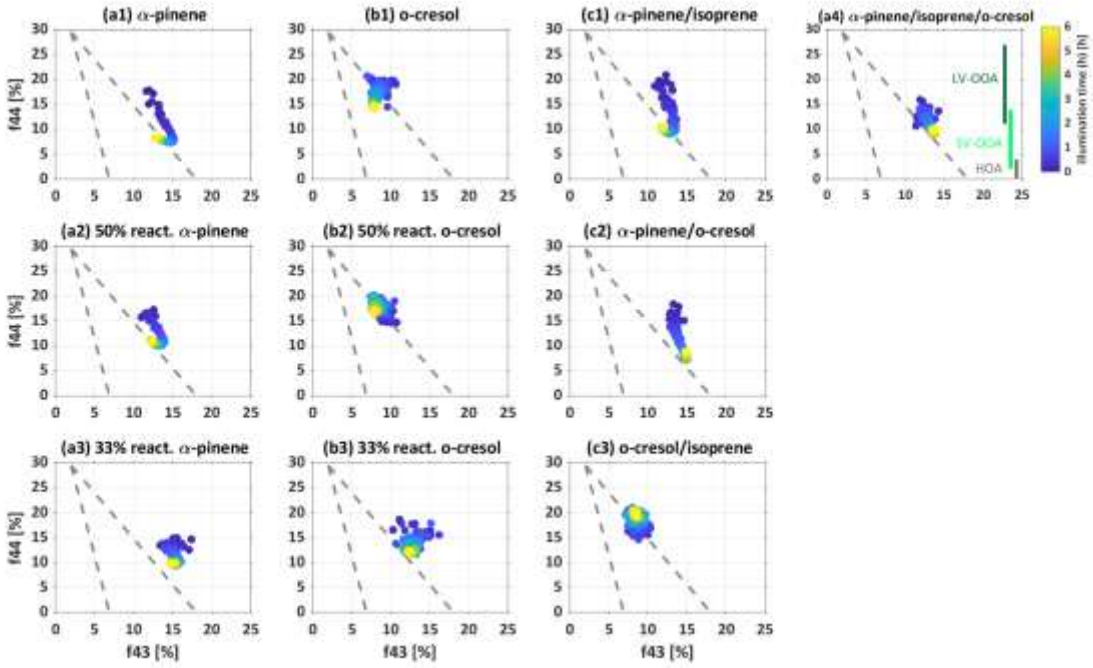

Figure S8: Trajectory of AMS f_{44} vs f_{43} in all investigated systems re-expressing the data in S7 following the approach of Ng et al. (2010). The colour represents the illumination time and the delineated triangular area broadly brackets ambient atmospheric compositional behaviour. The systems all fall to the right of the ambient area, particularly at the earlier stages – a finding frequently observed in many chamber systems (see e.g. Figure 4 in Alfarra et al., 2013).

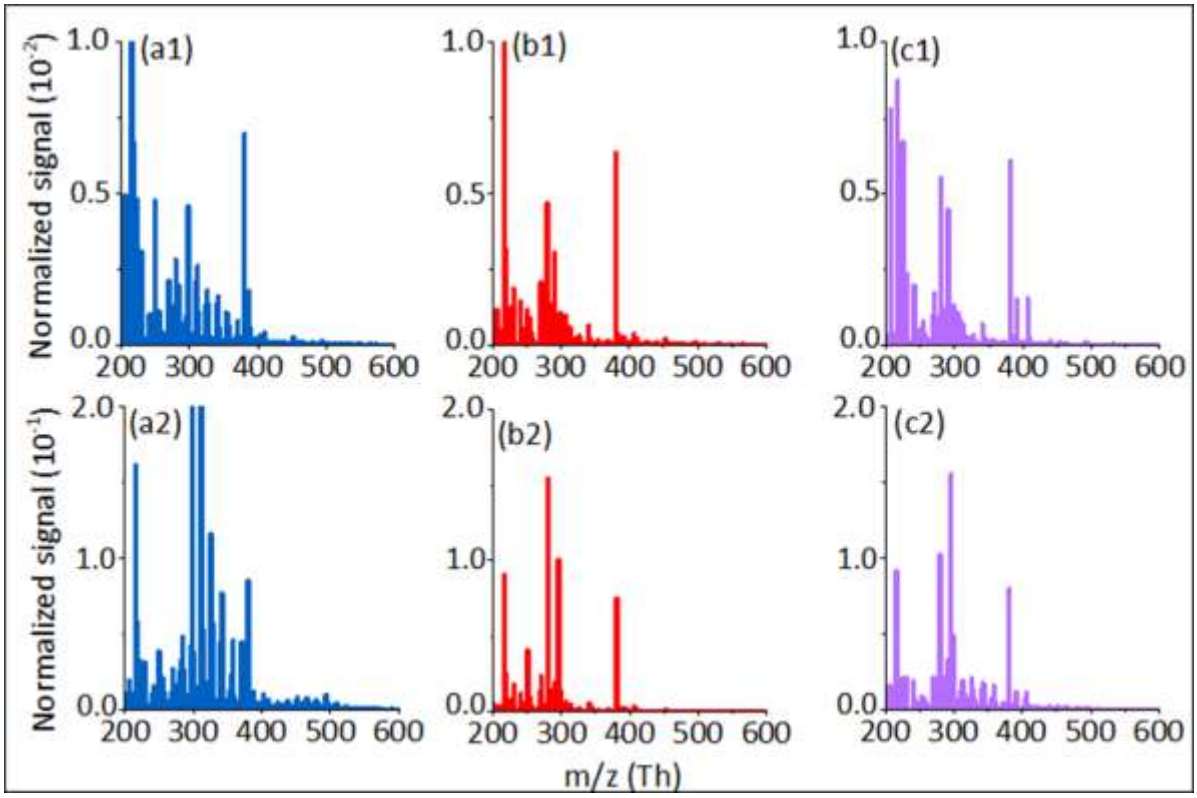

Figure S9: FIGAERO-I$^-$-CIMS particle-phase mass spectra taken in the single precursor *α*-pinene (a1 and a2), o-cresol (b1 and b2) and mixed *α*-pinene / o-cresol systems (c1 and c2) at 0.5 hour (a1, b1 and c1) and 5.5 hours (a2,b2 and c2) after the onset of photochemistry in the MAC. These mass spectra have been normalised to the same reagent ion (I^-) concentration. Noting the increase in the y-axis range in the bottom row, there is a clear increasing signal in the m/z range from 200 to 600 (I^--adducts) in all systems corresponding to the increase in measured particulate signal with the increase in SOA particle mass with time. Additionally, some peaks (e.g., m/z 358, 403, 419, 439, etc) are uniquely detected in the mass spectra of the mixture.

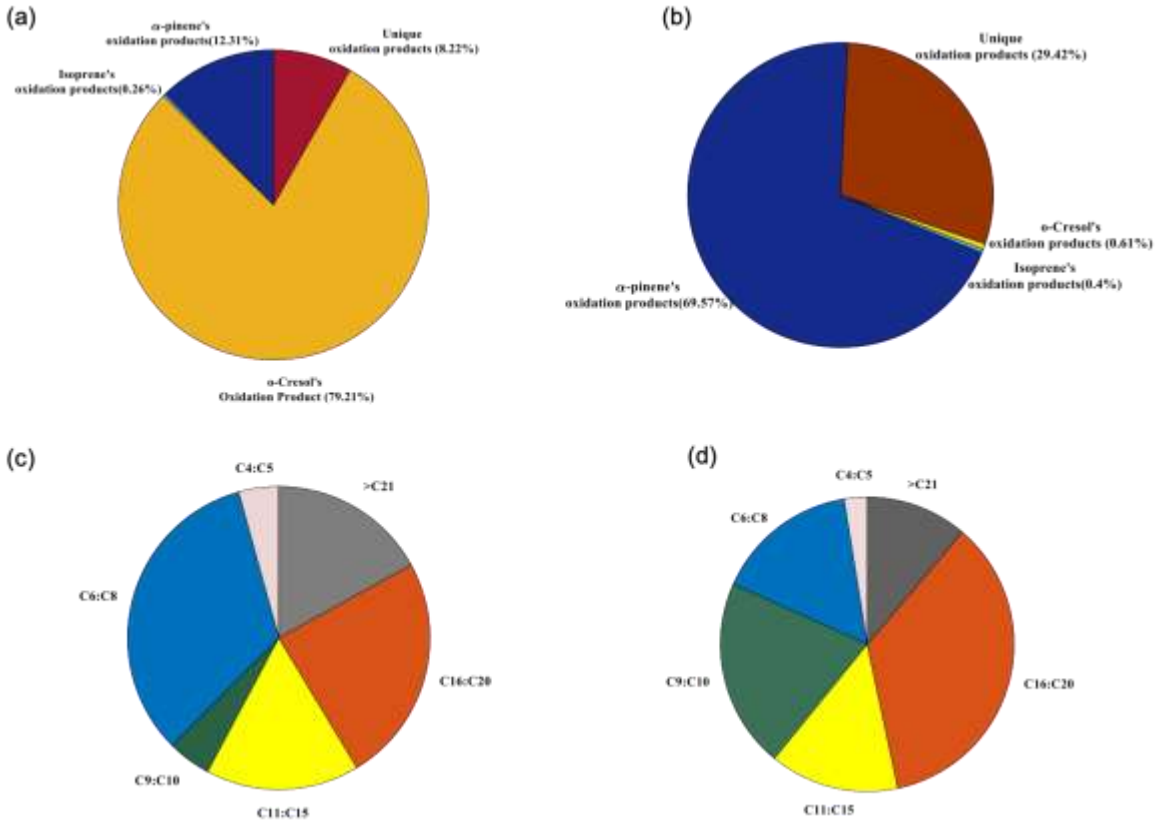

Figure S10: Molecular resolved compounds in the particle phase for the ternary *o*-cresol / *α*-pinene / isoprene mixture obtained using UPLC-Orbitrap MS of filter extracts: a) fraction of signal in negative mode, b) fraction of signal in positive mode, c) fraction of signal by carbon number in compounds uniquely found in the mixture in negative mode, d) fraction of signal by carbon number in compounds uniquely found in the mixture in positive mode.

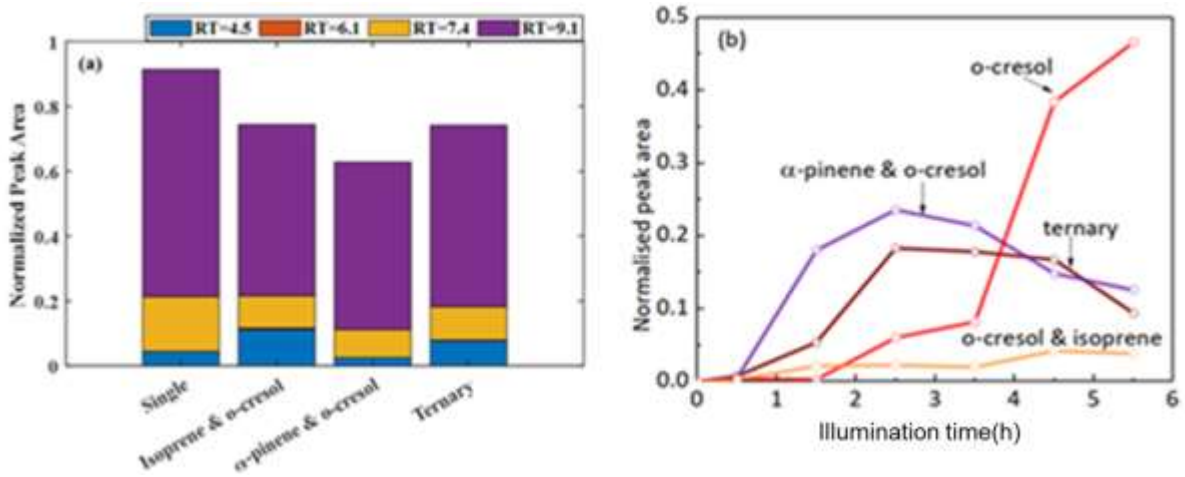

Figure S11: a) Normalised signal peak area of $C_7H_7NO_4$ isomers of filter extracts of particles in each o-cresol containing system from LC-Orbitrap MS analysis collected at the end of each experiment; b) time series of total particulate $C_7H_7NO_4$ (total signal at m/z=296) from FIGAERO-I^--CIMS. The peak area of the compound is normalised to the total peak area of all detected compounds from each instrument, respectively.

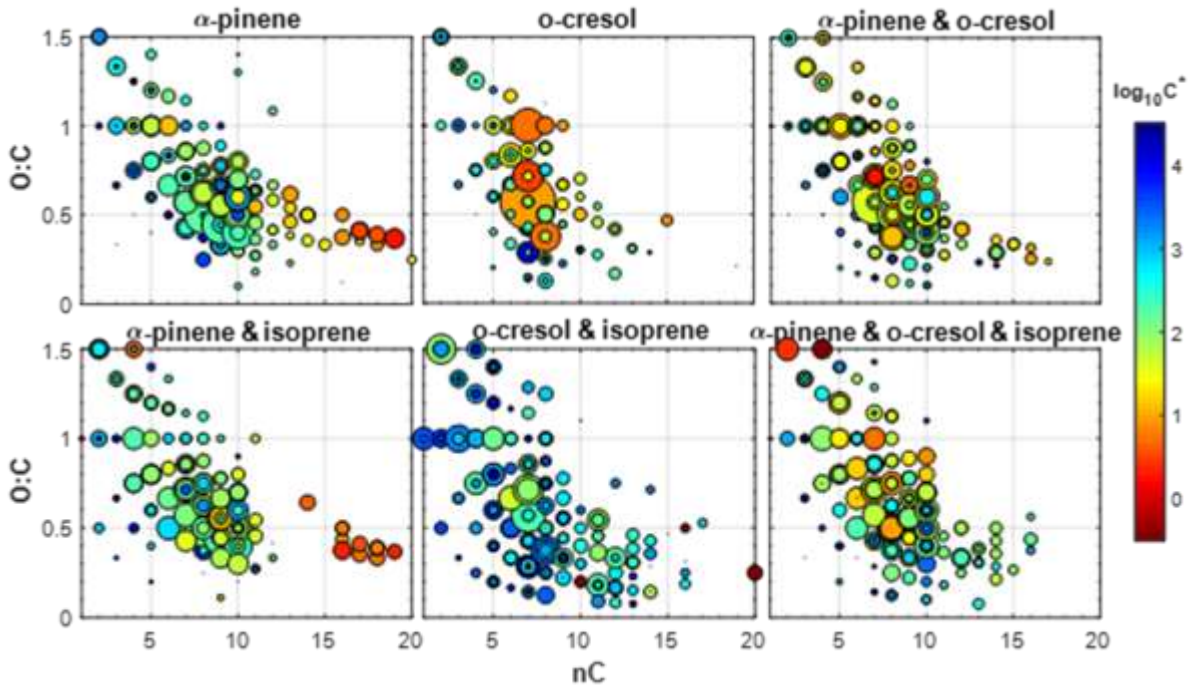

Figure S12: Oxygen to carbon ratio (O:C) vs carbon number (nC) of all the products identified by the FIGAERO-I^--CIMS in the particle phase at the end of each experiment in characteristic experiments in each system. The area of the symbol is proportional to the square root of the contribution of each product to the total signal and coloured according to their effective saturation concentration (C*). The C* was calculated using the gas to particle ratio of each ion and absorptive partitioning calculations. The FIGAERO-CIMS signals in both gas and particle phases were converted into concentrations (ions m^{-3}) based on the signal strength and the volume of air sampled. Using the fraction of each species in the particle phase (i.e., partitioning coefficient) and the total absorptive mass (in this case the total organics concentration), the saturation concentration of each identified product was calculated (see Donahue et al., 2006).

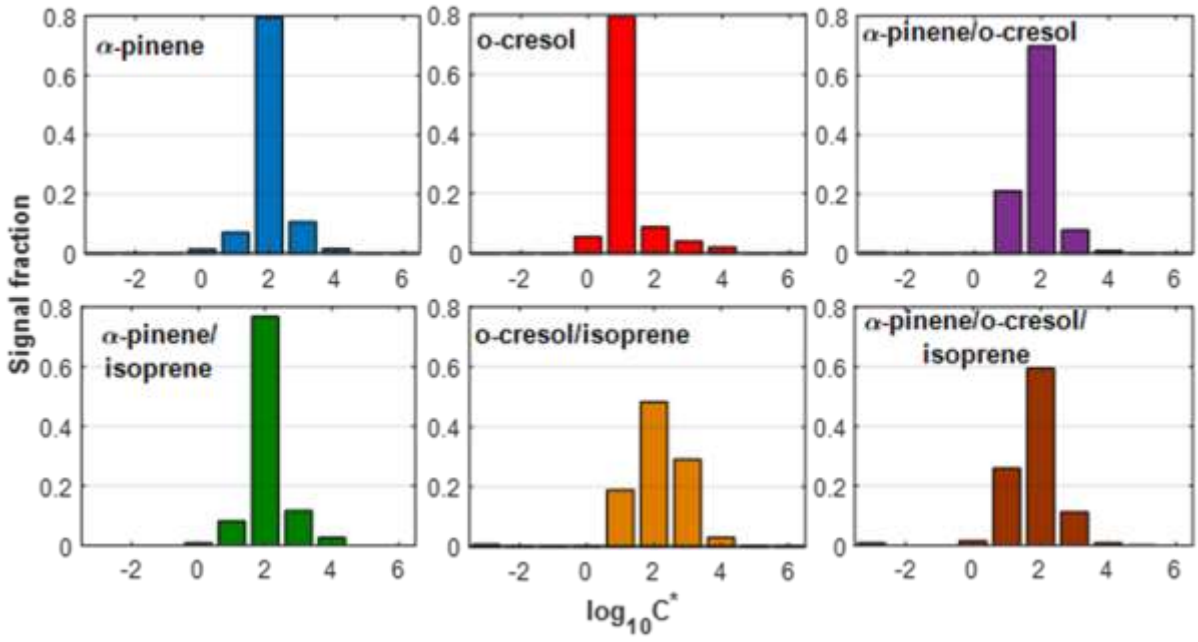

Figure S13: Volatility distributions expressed as effective saturation concentration (C*) in the volatility basis set framework of all the products identified by the FIGAERO-CIMS as a function of the total particle phase signal in example experiments in all systems. The C* was calculated using the gas to particle ratio of each of the identified species and absorptive partitioning calculations (see Fig. S12). The volatility derived from the FIGAERO-CIMS showed particularly narrow distributions, mainly dominated by semi-volatile organic compounds. Here, it can be seen that the volatility distributions of particles in the mixture experiments can be similar (α-pinene / isoprene) or quite different (o-cresol/isoprene) to those in the experiments using a single precursor. These observations suggest that the effect of mixing precursors can have a varying effect on the resultant particle volatility.

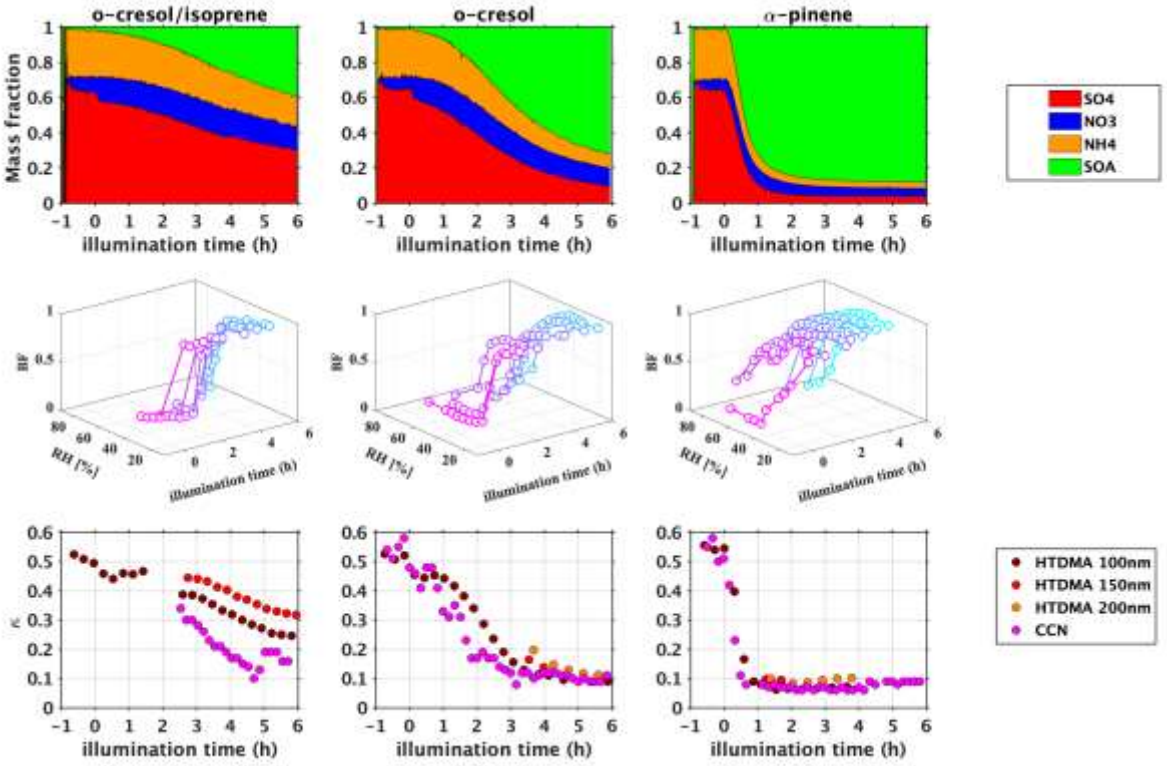

Figure S14: top row: the time series of AMS chemical composition in three exemplified systems. The SOA mass fraction change increases fastest in α-pinene systems and lowest in the *o*-cresol / isoprene system. Middle row: the corresponding time series of Bounce (or Rebound) Fraction (BF) at different RH between 20-85%. The transition RH from non-liquid (BF>0.8) to liquid phase (RH<0.2) increases with increasing SOA mass fraction. Bottom row: the corresponding time series of the hygroscopicity parameter, κ, measured under subsaturated (HTDMA, measured sizes increased with time through an experiment as particle sizes increased) and supersaturated (CCN) conditions. The particles become less hygroscopic (decreasing κ) with increasing SOA mass fraction.

Table S1: Digital object identifiers (DOI) of all the data used in this study for the experiments listed on Table 1. TMC: total mass concentration (density=1 g cm^{-3}); TNC: total number concentration; nitrogen monoxide (NO), nitrogen dioxide (NO_2) and ozone (O_3) mixing ratios; total particle organics concentration (Org_{tot}); VOC decay fraction (VOC). .n.a. indicates data that were not available due to instrument failures.

Exp. No.	TMC, TNC, NO, NO2, O3	Org_{tot}	VOC
1	https://doi.org/10.25326/FFTE-ED96	https://doi.org/10.25326/0QTA-SM15	https://doi.org/10.25326/0QTA-SM15
2	https://doi.org/10.25326/3549-H353	https://doi.org/10.25326/GXV6-3646	n.a.
3	https://doi.org/10.25326/47M1-MN95	n.a.	
4	https://doi.org/10.25326/9WDC-BG18	https://doi.org/10.25326/5AJ0-6150	https://doi.org/10.25326/5AJ0-6150
5	https://doi.org/10.25326/AH45-9F95	https://doi.org/10.25326/VM0N-Q983	https://doi.org/10.25326/VM0N-Q983
6	https://doi.org/10.25326/59RG-Y252	https://doi.org/10.25326/3ATZ-0780	https://doi.org/10.25326/3ATZ-0780
7	https://doi.org/10.25326/GMZK-YX22	https://doi.org/10.25326/RNGC-1628	n.a.
8	https://doi.org/10.25326/4RKZ-H076	https://doi.org/10.25326/Y7RC-MK49	https://doi.org/10.25326/Y7RC-MK49
9	https://doi.org/10.25326/P1WB-1V56	n.a.	n.a.
10	https://doi.org/10.25326/Y275-K605	https://doi.org/10.25326/G0X4-TB38	https://doi.org/10.25326/G0X4-TB38
11	https://doi.org/10.25326/RB9Y-AF97	https://doi.org/10.25326/4XSN-AB47	n.a.
12	https://doi.org/10.25326/JDMS-ZR65	https://doi.org/10.25326/3WY2-D921	https://doi.org/10.25326/3WY2-D921
13	https://doi.org/10.25326/T6H3-JQ42	https://doi.org/10.25326/T6H3-JQ42	https://doi.org/10.25326/T6H3-JQ42
14	https://doi.org/10.25326/KP9S-F341	https://doi.org/10.25326/VTCR-KD24	https://doi.org/10.25326/VTCR-KD24
15	https://doi.org/10.25326/E0EP-QR41	https://doi.org/10.25326/GV1J-CE17	https://doi.org/10.25326/GV1J-CE17
16	https://doi.org/10.25326/4QB0-PE88	https://doi.org/10.25326/JBMD-1D11	https://doi.org/10.25326/JBMD-1D11
17	https://doi.org/10.25326/DPYJ-RE18	na	n.a.
18	https://doi.org/10.25326/4KH1-4152	https://doi.org/10.25326/7NBS-C877	https://doi.org/10.25326/7NBS-C877
19	https://doi.org/10.25326/E3WH-DX73	https://doi.org/10.25326/E3WH-DX73	https://doi.org/10.25326/E3WH-DX73
20	https://doi.org/10.25326/K0AA-1588	https://doi.org/10.25326/3GCH-NT90	n.a.
21	https://doi.org/10.25326/4909-6448	https://doi.org/10.25326/SY6A-H369	https://doi.org/10.25326/SY6A-H369
22	https://doi.org/10.25326/XE37-GC95	n.a.	https://doi.org/10.25326/5NXY-WN10
23	https://doi.org/10.25326/HNCK-KE85	https://doi.org/10.25326/28KM-B382	n.a.
24	https://doi.org/10.25326/1D6D-TQ82	https://doi.org/10.25326/P859-2T83	https://doi.org/10.25326/P859-2T83